Fluid–rigid Structure Interaction of Moving Cuttlefish Robot Using Moving Mesh Method

†*Shinichi ASAO[1], Masashi YAMAKAWA[2], and Yuto MORI[2]

[1]Department of Mechanical Engineering, College of Industrial Technology, Japan
[2]Department of Mechanical Engineering, Kyoto Institute of Technology, Japan

*Presenting author: asao@cit.sangitan.ac.jp
†Corresponding author: asao@cit.sangitan.ac.jp

Abstract

Cuttlefish are known to have superior characteristics for attitude control by using two fins. The objective of this study is to clarify the characteristics of cuttlefish-like motion for an optimal attitude control. To analyze both flows around a cuttlefish and its motion depending on fluid force, coupled simulation of the moving computational domain method and motion dynamics were applied. Furthermore, moving mesh techniques combined with a torsional spring approach and an angle-based-smoothing enabled the calculation of various fin motions. As a first step, it is confirmed whether fluid–rigid structure interaction of moving cuttlefish robot is correct. As a result of comparison with the movement of the experiment robot, the movement was almost in agreement. Therefore, this calculation method is effective. In addition, it was found that the influence of the movement of cuttlefish fins on the flow field was small.

Keywords: Cuttlefish, moving boundary problem, moving mesh method

Introduction

Cuttlefish swim by undulating the fins on the sides of their bodies. This affects the surrounding flow and enables fine movement, resulting in excellent attitude control. By incorporating this movement into a fish-type robot, the robot can move underwater without raising mud on the sea floor or getting entangled in seaweed. The robot can also achieve fine attitude control when working with its arms.

The way cuttlefish swim is currently being studied. Kier et al. [1] suggested that in their fin movements, cuttlefish swim in almost the same way as do fish. Rahman et al. [2] are developing a robot that imitates the side fins of cuttlefish. They have indicated that propulsion and rotation can be performed by fin undulation. However, little has been reported on attitude control. Enabling a robot to achieve attitude control will make it possible to smoothly perform underwater work and ecological surveys even if disturbances such as tidal currents and waves largely affect the obtained results. It is therefore important to conduct research on the attitude control mechanism. Although experiments have been done using a robot, they are costly and difficult to implement. Therefore, studies based on numerical fluid dynamics are effective. On the other hand, as a simulation method, it is necessary to consider the interaction of moving fins and fluid flow around the fins and body. Therefore, we performed a coupled simulation of fluid dynamics and dynamics of structure.

In the work we report in this paper, we clarified fin movement as a means to achieve attitude control and performed coupled simulation of numerical fluid dynamics and structure

dynamics. As a first step, we determined whether the fluid–rigid structure interaction of a moving cuttlefish robot is correct.

NUMERICAL APPROACH

Governing equations

The governing equations are the continuity equation and the incompressible Navier–Stokes equation. These are written as

$$\nabla \cdot \boldsymbol{q} = 0, \tag{1}$$

$$\frac{\partial \boldsymbol{q}}{\partial t} + \frac{\partial \boldsymbol{E}_a}{\partial x} + \frac{\partial \boldsymbol{F}_a}{\partial y} + \frac{\partial \boldsymbol{G}_a}{\partial z} = -\left(\frac{\partial \boldsymbol{E}_p}{\partial x} + \frac{\partial \boldsymbol{F}_p}{\partial y} + \frac{\partial \boldsymbol{G}_p}{\partial z} \right) + \frac{1}{\mathrm{Re}} \left(\frac{\partial \boldsymbol{E}_v}{\partial x} + \frac{\partial \boldsymbol{F}_v}{\partial y} + \frac{\partial \boldsymbol{G}_v}{\partial z} \right), \tag{2}$$

where $\boldsymbol{q}$ is the velocity vector, $\boldsymbol{E}_a$, $\boldsymbol{F}_a$, and $\boldsymbol{G}_a$ are respectively advection flux vectors in the x, y, and z directions, $\boldsymbol{E}_v$, $\boldsymbol{F}_v$, and $\boldsymbol{G}_v$ are viscous-flux vectors, and $\boldsymbol{E}_p$, $\boldsymbol{F}_p$, and $\boldsymbol{G}_p$ are pressure terms. The elements of the velocity vector and flux vectors are

$$\begin{gathered}
\boldsymbol{q} = \begin{bmatrix} u \\ v \\ w \end{bmatrix}, \boldsymbol{E}_a = \begin{bmatrix} u^2 \\ uv \\ uw \end{bmatrix}, \boldsymbol{F}_a = \begin{bmatrix} uv \\ v^2 \\ vw \end{bmatrix}, \boldsymbol{G}_a = \begin{bmatrix} uw \\ vw \\ w^2 \end{bmatrix}, \\
\boldsymbol{E}_p = \begin{bmatrix} p \\ 0 \\ 0 \end{bmatrix}, \boldsymbol{F}_p = \begin{bmatrix} 0 \\ p \\ 0 \end{bmatrix}, \boldsymbol{G}_p = \begin{bmatrix} 0 \\ 0 \\ p \end{bmatrix}, \\
\boldsymbol{E}_v = \begin{bmatrix} u_x \\ v_x \\ w_x \end{bmatrix}, \boldsymbol{F}_v = \begin{bmatrix} u_y \\ v_y \\ w_y \end{bmatrix}, \boldsymbol{G}_v = \begin{bmatrix} u_z \\ v_z \\ w_z \end{bmatrix}
\end{gathered} \tag{3}$$

where u, v, and w are respectively the velocity components of the x, y, and z directions and p is pressure. The x, y, and z subscripts respectively indicate derivatives derived from x, y, and z and Re is the Reynolds number. We also took into account the combined translation and rotation motions of a cuttlefish. The rigid body equations of motion are

$$\frac{d\boldsymbol{p}_B}{dt} = \boldsymbol{f}_B \tag{4}$$

$$\frac{d\boldsymbol{L}_B}{dt} + \omega_B \times \boldsymbol{L}_B = \boldsymbol{N}_B \tag{5}$$

Here, $\boldsymbol{p}_\mathrm{B}$ is the momentum vector of the body, $\boldsymbol{f}_\mathrm{B}$ is the external force vector, $\boldsymbol{L}_\mathrm{B}$ is the angular momentum vector, $\boldsymbol{N}_\mathrm{B}$ is the torque vector, and ω_B is the angular velocity.

Moving-grid finite-volume method

To ensure the geometric conservation laws are followed, we used a control volume in the space-time unified domain (x, y, z, t), which is four-dimensional in the case of three-dimensional flows. This enables Eq. (2) to be written in divergence form as

$$\tilde{\nabla} \cdot \tilde{\boldsymbol{F}} = \boldsymbol{0}, \tag{6}$$

where

$$\tilde{\nabla} = \begin{bmatrix} \dfrac{\partial}{\partial x} \\ \dfrac{\partial}{\partial y} \\ \dfrac{\partial}{\partial z} \\ \dfrac{\partial}{\partial t} \end{bmatrix}, \quad \tilde{\boldsymbol{F}} = \begin{bmatrix} \boldsymbol{E}_a + \boldsymbol{E}_p - \dfrac{1}{\mathrm{Re}}\boldsymbol{E}_v \\ \boldsymbol{F}_a + \boldsymbol{F}_p - \dfrac{1}{\mathrm{Re}}\boldsymbol{F}_v \\ \boldsymbol{G}_a + \boldsymbol{G}_p - \dfrac{1}{\mathrm{Re}}\boldsymbol{G}_v \\ \boldsymbol{q} \end{bmatrix}. \tag{7}$$

The present method is based on a cell-centered finite-volume method. Thus, the flow variables are defined at the center of the cell in the (*x*, *y*, *z*) space. The control volume becomes a four-dimensional polyhedron in the (*x*, *y*, *z*, *t*)-domain, as schematically illustrated in Figure 1.

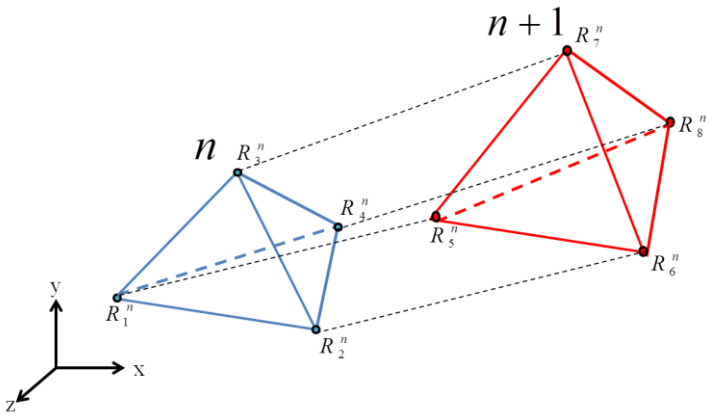

Figure 1 Schematic view of control volume $\tilde{\Omega}$ in (*x*, *y*, *z*, *t*) space-time unified domain.

We apply volume integration to Eq. (6) with respect to the control volume illustrated in Figure 1. Using the Gauss theorem, we can write Eq. (6) in surface integral form as

$$\int_{\tilde{\Omega}} \tilde{\nabla} \cdot \tilde{\boldsymbol{F}} \mathrm{d}\tilde{V} = \oint_{\partial\tilde{\Omega}} \tilde{\boldsymbol{F}} \cdot \tilde{\boldsymbol{n}}_u \mathrm{d}\tilde{S} \approx \sum_{l=1}^{6} \left(\tilde{\boldsymbol{F}} \cdot \tilde{\boldsymbol{n}} \right)_l = \boldsymbol{0} \tag{8}$$

Here, $\tilde{\boldsymbol{n}}_u$ is an outward unit vector normal to the surface of the polyhedron control volume $\tilde{\Omega}$ ($\partial\tilde{\Omega}$). The term $\tilde{\boldsymbol{n}} = (\tilde{n}_x, \tilde{n}_y, \tilde{n}_z, \tilde{n}_t)_l$, ($l$=1, 2,... 6) denotes the surface normal vector of control volume and its length is equal to the boundary surface area in four-dimensional (*x*, *y*, *z*, *t*) space. The upper and bottom boundaries of the control volume (l = 5 and 6) are perpendicular to the *t*-axis. Therefore they have only the $\tilde{n}_t$ component, the length of which corresponds respectively to the cell volume in the (*x*, *y*, *z*)-space at time t^n and t^{n+1}. Thus, Eq. (8) can be expressed as

$$\boldsymbol{q}^{n+1}(\tilde{n}_t)_6 + \boldsymbol{q}^{n}(\tilde{n}_t)_5 + \sum_{l=1}^{4}\left(\tilde{\boldsymbol{F}}\cdot\tilde{\boldsymbol{n}}\right)_l^{n+1/2} = \boldsymbol{0}. \tag{9}$$

Moving computational domain method

The basic coordinate system of the moving computational domain method is the general, fixed, stationary (x, y, z) Cartesian coordinate system. The computational domain itself, including the body inside, moves in the fixed (x, y, z)-space. The flow around the body is calculated as the moving boundary problem. Unknown flow variables, such as pressure p and x-directional velocity u, are defined at each grid cell center in the computational domain. The motion of the computational domain in accordance with the body motion y in the physical space is arbitrary. Accordingly, any kind of body motion can be simulated by the moving computational domain method. The flow field driven by the body is calculated in the computational domain in which the body fitted mesh system is used. The computational domain itself moves in the physical (x, y, z) space time-dependently. Thus, since the mesh system of the computational domain also moves in the (x, y, z) space, a flow solver has to be constructed for the moving grid system. In the present moving computational domain method, the moving-grid finite-volume method [3] is used. The only necessary and essential assumption is that the conditions in front of the moving computational domain have to be known because they are necessary as a boundary condition of the flow solver. The natural assumption may be the stationary fluid condition in front of the moving computational domain.

Spring approach for moving grid

Cuttlefish fins change their angle from 0 to 45 degrees. To express such fin movements, it is necessary to use a large movement defined by a computational grid. Thus, we used the spring approach [4], which adds a torsion spring effect to the conventional spring method. In this approach, to obtain robustness in the computation, we added a spring constant associated with the shape of the cell (cells sides' angles), as shown in Equation (10).

$$k_{ij} = k_{[spring]ij} + k_{[angle]ij} \tag{10}$$

In our work, we specifically used the following equations:

$$k_{[spring]ij} = \frac{1}{l_{ij}^2} \tag{11}$$

$$k_{[angle]ij} = \sum \frac{1}{\sin^2\theta_{in}} + \sum \frac{1}{\sin^4\theta_{dn}}, \tag{12}$$

where l_{ij} shows the side length of the cell. Then, θ_{in} and θ_{di} are angles defined by two torsion sides of a tetrahedral cell, as shown in Figure 2.

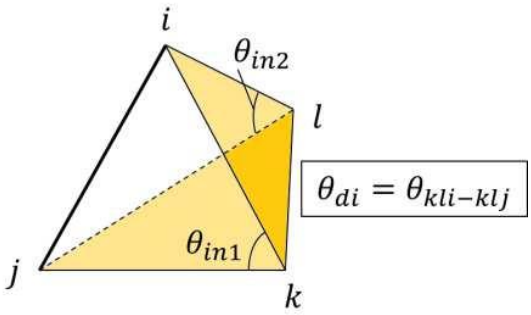

Figure 2 Spring constant for tetrahedron.

Numerical procedure

To solve Eq. (9), we apply the SMAC method [5]. Thus, Eq. (9) can be solved in the three following stages. The equation to be solved at the first stage contains unknown variables at n+1-time step in flux terms. Thus, the equation is iteratively solved using the LU-SGS method [6]. The equation to be solved at the second stage is the Poisson equation about the pressure correction. This equation is iteratively solved using the Bi-CGSTAB method [7]. The flux vectors are evaluated using the QUICK method, whereas the flux vectors of the pressure and viscous terms are evaluated in a central-difference-like manner. The incompressible fluid-body interaction is calculated in the first step of the SMAC method. Figure 3 shows the flowchart of the fluid-body interaction.

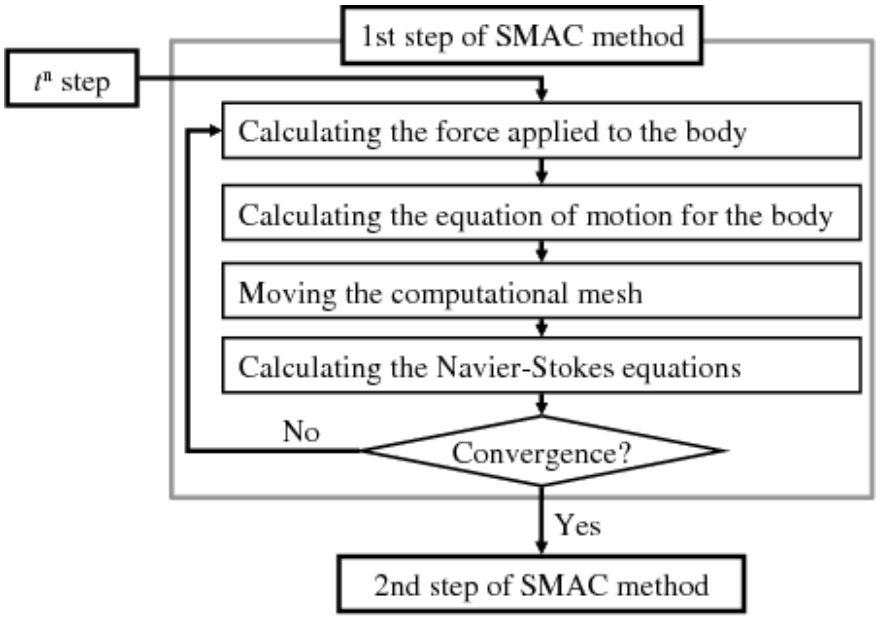

Figure 3 Flowchart for interaction calculation.

NUMERICAL RESULTS

To verify the efficacy of the fluid–rigid structure interaction method, we used a cuttlefish robot to compare simulation results with the experiment results [2]. In the experiment, we

investigated circular movement due to the frequency differences between the left and right fins.

Calculation model

The experiment robot used in this calculation is shown in Figure 4. The robot has a total length of 1.3 m, a maximum width of 0.714 m, a thickness of 0.1 m, a fins length of 0.874 m, a fillet width of 0.075 m and a weight of 62.8 kg.

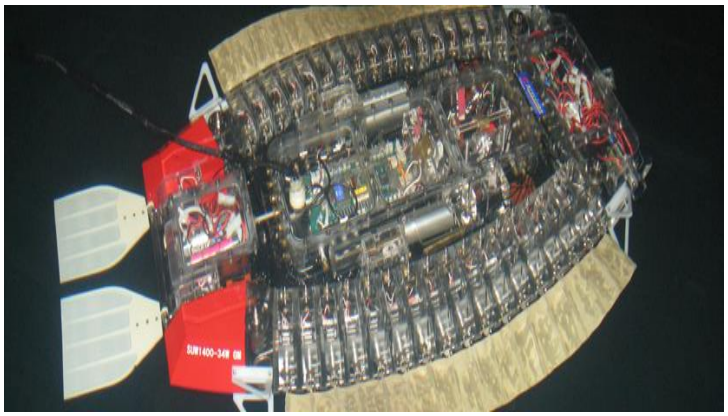

Figure 4 Cuttlefish robot [2].

The calculation model is shown in Figure 5. On a dimensionless basis, its total length L amounts to the total length of the experiment robot. Figure 6 shows the model's surface mesh and Figure 7 shows the computational mesh around the model. We generated the computational mesh using MEGG3D supported by JAXA [8]. The calculation region is a sphere with diameter $30L$. The number of cells is 2,875,222. The coordinate system defines the x axis in the length direction and the y axis in the width direction, and the direction perpendicular to them is the z axis.

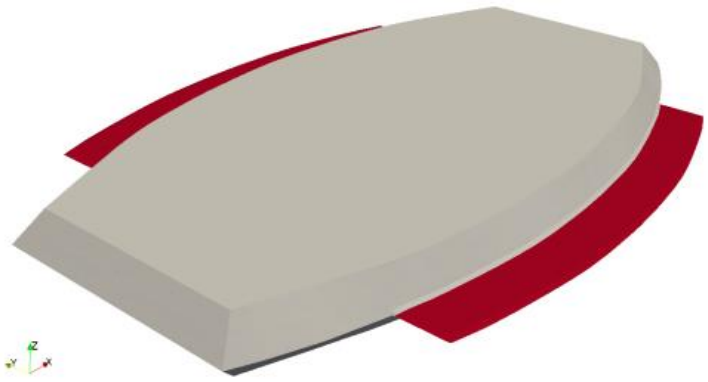

Figure 5 Cuttlefish robot model.

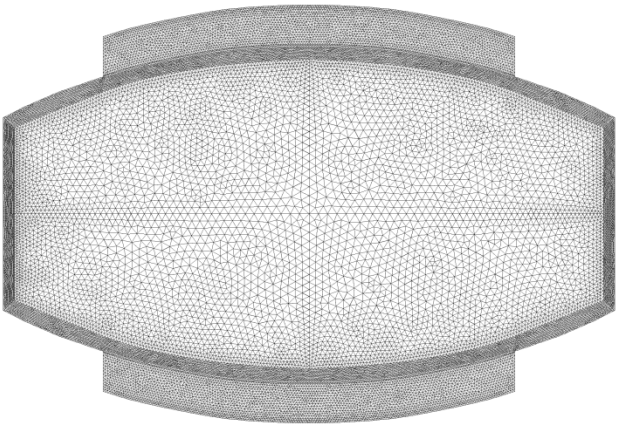

Figure 6 Cuttlefish robot surface mesh.

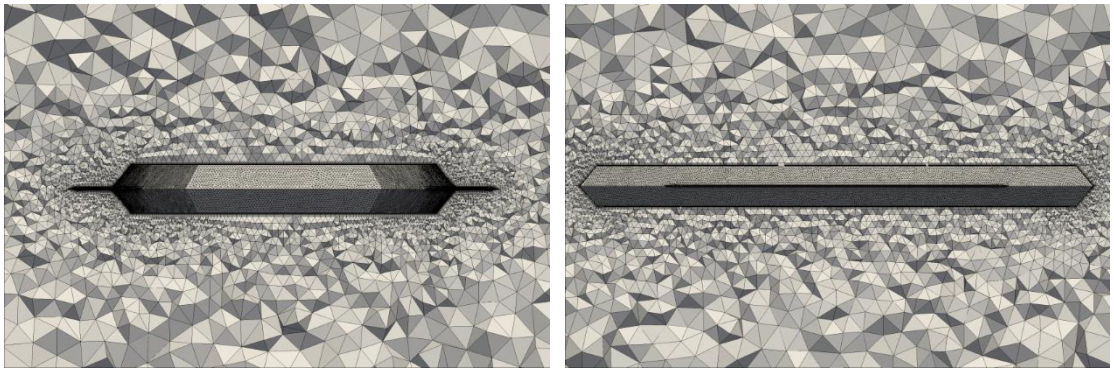

(a) *y*-*z* plane (b) *x*-*z* plane

Figure 7 Computational mesh around cuttlefish robot.

Fin movements

The cuttlefish fins move in a traveling wave motion and the fin deformation is represented by the following equations:

$$\theta = \Theta(s)\sin(2\pi Ks - 2\pi Nt), \tag{13}$$

$$\Theta(s) = \sin^{-1}\left[\left\{1 - 0.905\left(\frac{s}{fL} - 0.5\right)^2\right\}\sin\theta_{\max}\right], \tag{14}$$

$$y(t) = r\cos\theta, \tag{15}$$

$$z(t) = r\sin\theta. \tag{16}$$

In these equations, θ is the angle from the base of the fin to its tip, K is wave number, N is frequency, fL is the fin length in the x direction, s is the length in the x direction from the tip of the fillet, $\theta_{\max}$ is the maximum angle, and r is the length from the base of the fins to the tip. In accordance with the experiment conditions, the calculation condition was set to 1 for the wave number and 45° for the maximum angle. The direction of traveling wave motion is the-x direction. The left and right fins are defined as shown in Figure 8. The left fin frequency is 0.5 Hz and the right fin frequency is 1.0 Hz.

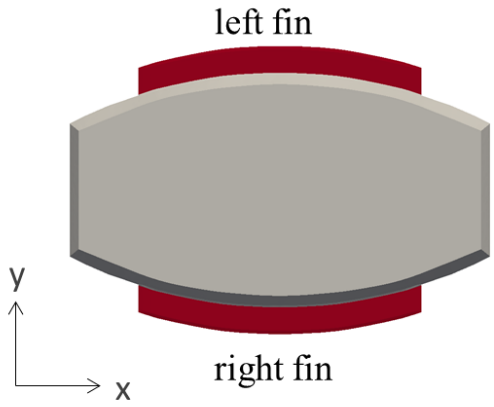

Figure 8 Definition of robot's left and right fins.

Movement and deformation of computational mesh

Figure 9 shows the movement and deformation of the space mesh. This figure shows that the fin movement is represented by the deformation of the computational mesh and the quality of the cell shape is maintained.

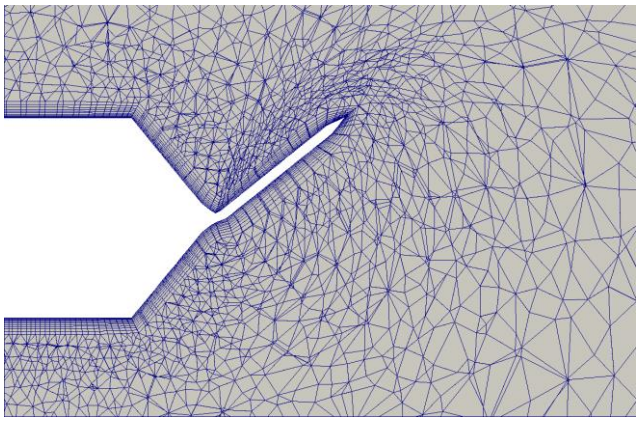

(a) Fin angle: 45 degrees

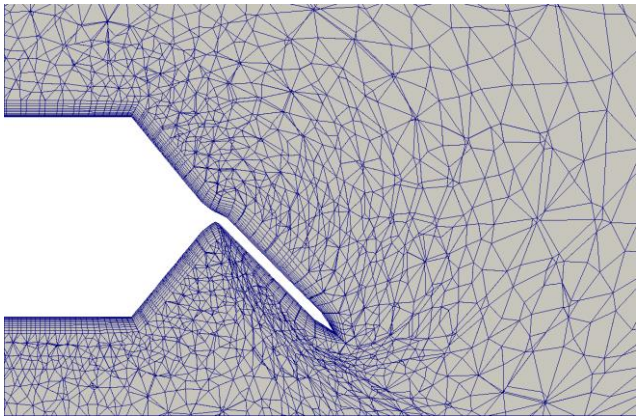

(b) Fin angle: -45 degrees

Figure 9 Mesh deformation for fin motion at *y*-*z* plane.

Calculation conditions

As computational conditions, the characteristic length is 1.3 m, the characteristic velocity is 0.5 m/s, the kinematic viscosity of water is 1.004×10^{-6} m^2/s, and the Reynolds number is 647,000. The time step is 0.0001. It is assumed that the model moves in static fluid. The initial stationary condition of pressure and the velocity components in the *x*, *y*, and *z* directions are given by p = 0.0 and $u = v = w = 0.0$. The model movements are obtained by coupled analysis of fin movement and fluid dynamics.

Trajectory of moving cuttlefish robot

Figure 10 shows the movement trajectory of the side fin type robot up to $T = 51.4$ s. This figure shows the trajectory from the upper side, and the one that is not transparent is the position at $T = 51.4$ s. The robot gradually rotates in the acceleration from the stationary state and performs the circular movement. The obtained results confirmed that the simulation reproduces the movement in which the speed and the attitude angle change moment by moment.

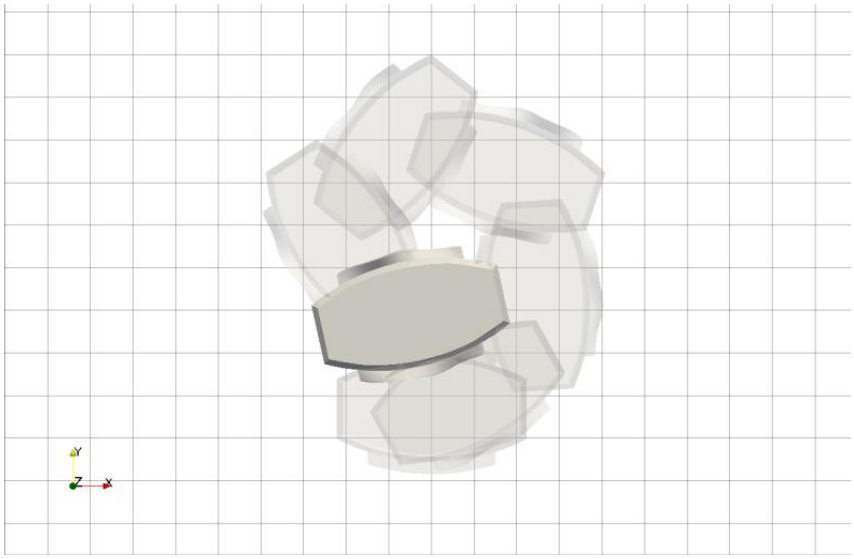

Figure 10 Trajectory of cuttlefish robot in circular motion.

We used the calculation results to compare the gravity position center coordinates of the robot obtained in the experiment Rahman et al. reported [2]. Figure 11 shows a comparison of the trajectory of the center of gravity position in the *x*-*y* plane. Red lines represent simulation results and blue lines represent experimental results. Figure 11 shows that both trajectories have the same circular motion. In comparing the circular motion diameters, we found the experimental result was 1.40 m, the simulation result was 1.31 m, and the error was 6.8%. The simulation result and the experimental result basically match. This confirms the effectiveness of the present calculation method of fluid-rigid structure interaction and the validity of the calculation result.

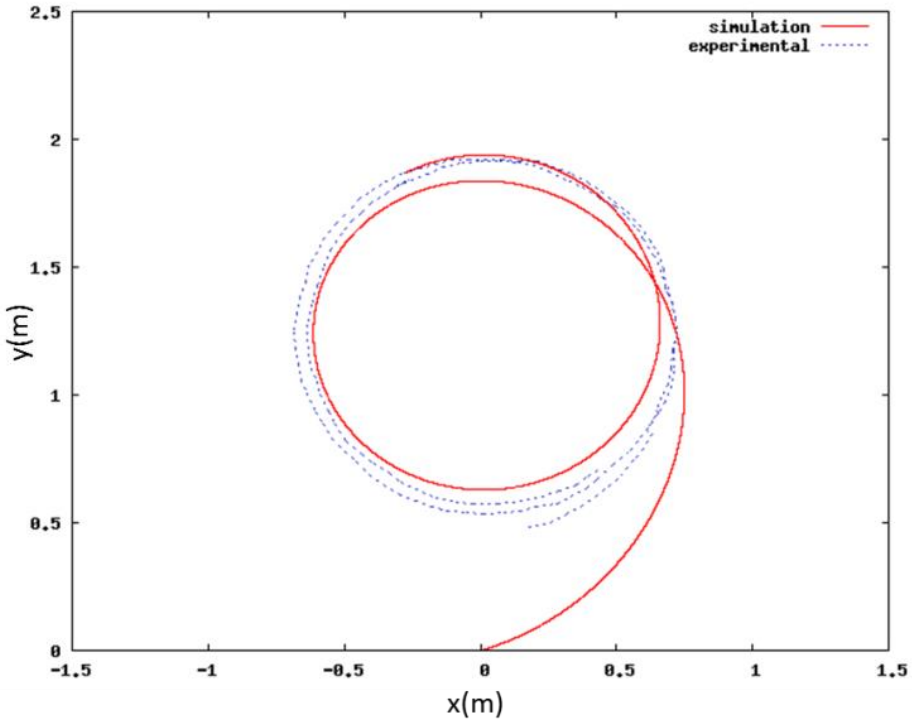

Figure 11 Center of gravity trajectory.

The flow field calculation results we obtained were a 0.1 m/s velocity isosurface around the robot at t = 0 s, 17.1 s, 34.3 s, and 51.4 s (Figure 12). We consider that the velocity isosurface exist only around the fins, which little affects the surrounding flow. Figure 13 shows the pressure distribution on the cuttlefish robot surface. The obtained results confirm that in frequency terms the pressure changes more in the right fins than in the left fins, and that thus a difference in thrust force exists between the left and right fins.

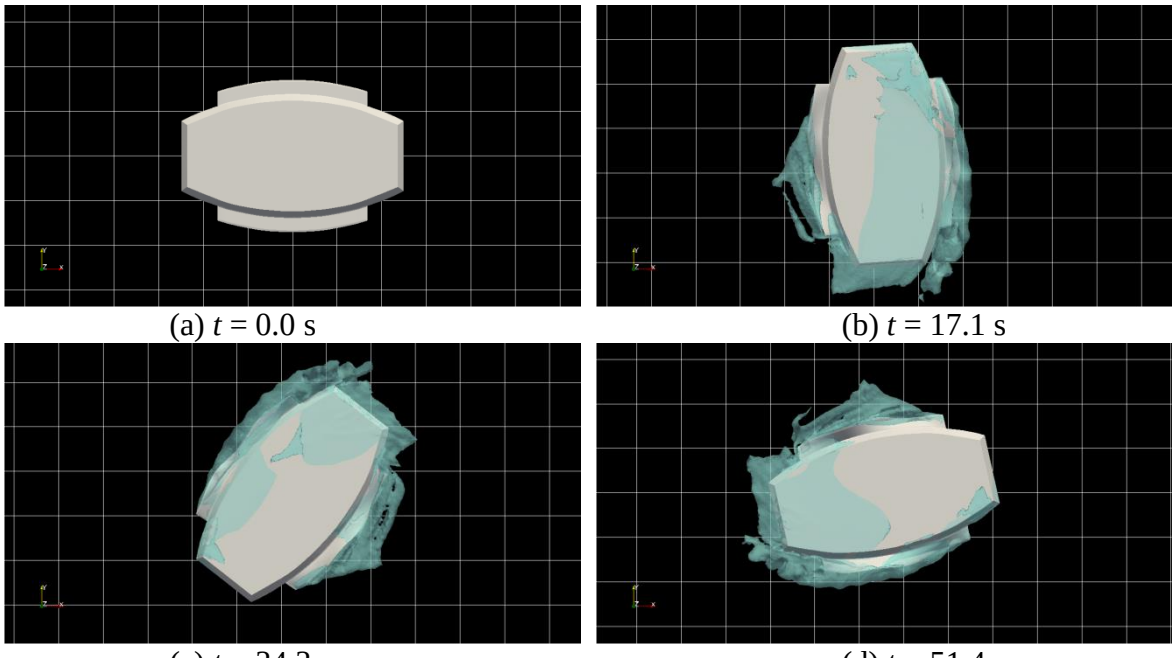

(a) t = 0.0 s (b) t = 17.1 s

(c) t = 34.3 s (d) t = 51.4 s

Figure 12 Velocity isosurface at V = 0.1 m/s

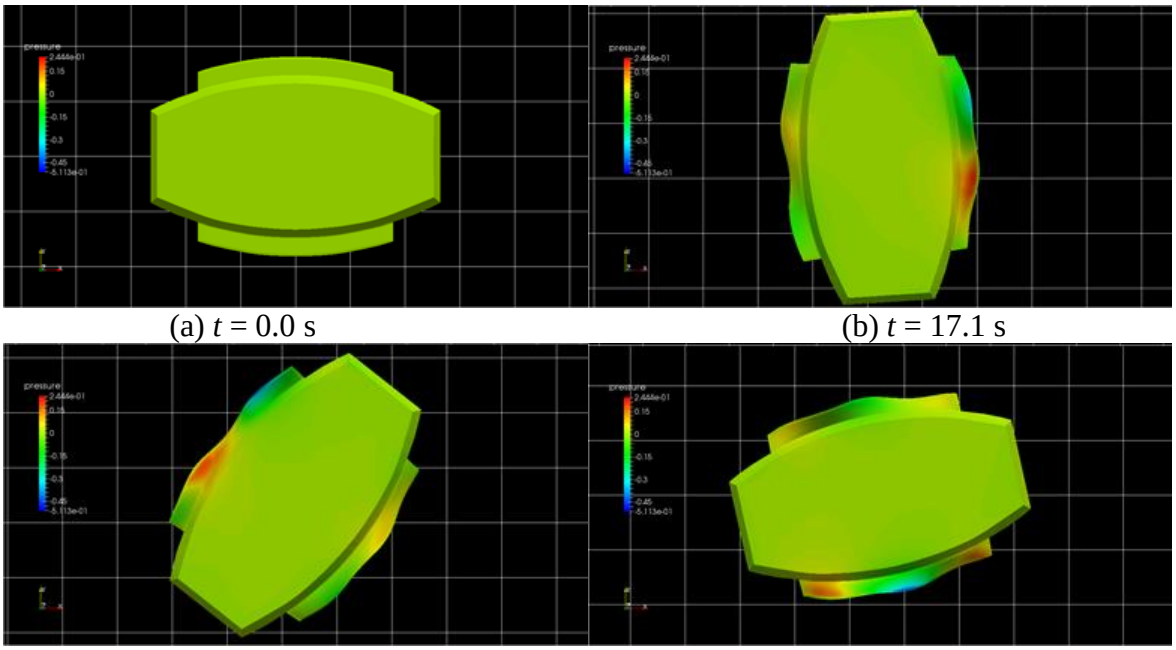

(a) t = 0.0 s (b) t = 17.1 s

(c) t = 34.3 s (d) t = 51.4 s

Figure 13 Pressure distribution on the cuttlefish robot surface.

Figure 14 shows the time history of the forces applied to the whole object, i.e. the right and left fins in the x direction. These x directions refer to the object fixed coordinate system. Figure 14 shows that a propulsion force applied to the right fin is larger than that applied to the left fin. The difference in the thrust force applied to the left and right fins makes a circular motion.

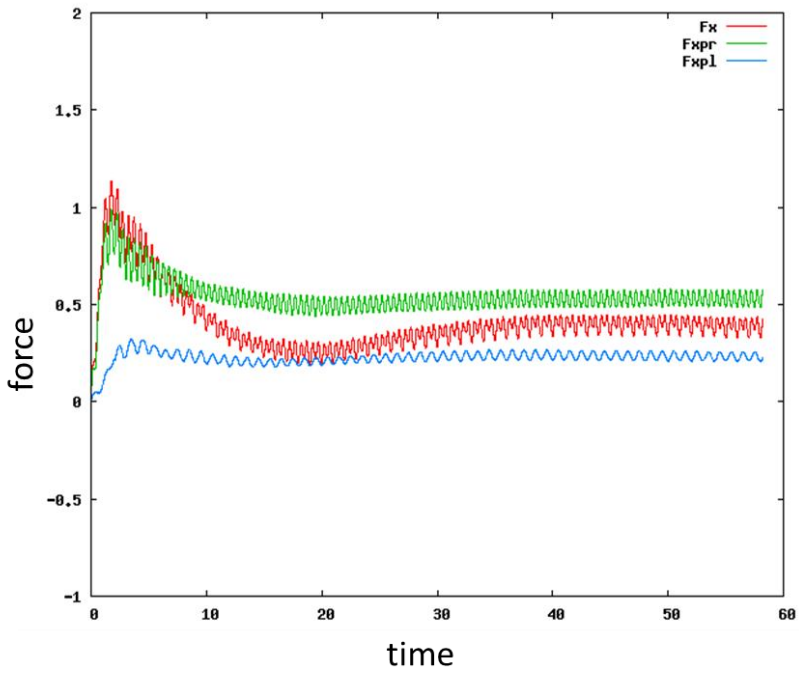

Figure 14 Time history of force applied to the robot.

CONCLUDING REMARKS

We confirmed whether fluid–rigid structure interaction of a moving cuttlefish robot was correct for attitude control. In comparing experiment results with calculation results, we found that they agreed well. We ascertained that the calculation method results obtained with our method agreed well with simulation results and showed our method's efficacy. We also confirmed that the fin movement did not affect the flow field very significantly. We also found that the difference in thrust force on the left and right fins makes a circular motion.

Acknowledgements

This publication was subsidized by JKA through its promotion funds from KEIRIN RACE, and by JFE 21st Century Foundation.

References

[1] S. Johnsen and W. M. Kier, Intramuscular crossed connective tissue fibres: skeletal support in the lateral fins of squids and cuttlefish, Department of Biology, Land, 231, pp. 311–338, DOI: 10.1111/j.1469-7998.1993.tb01921.x (1993).

[2] M. M. Rahman, H. Miki, S. Sugimori, Y. Sanada, and Y. Toda, Development of a Real Time Simulator Based on the Analysis of 6-Degrees of Freedom Motion of a Biomimetic Robot with Two Undulating Side Fins. Journal of Aero Aqua Bio-mechanisms. 3 (1), pp. 71–78, DOI: 10.5226/jabmech.3.71 (2013).

[3] M. Yamakawa and K. Matsuno, An Iterative Finite-Volume Method on an Unstructured Moving Grid: 1st Report, The Fundamental Formulation and Validation for Unsteady Compressible Flows, JSME, Series B, Vol. 69-683, pp. 1577–1582, DOI: 10.1299/kikaib.69.1577 (2003).

[4] G. A. Markou, Z. S. Mouroutis, D. C. Charmpis, and M. Papadrakakis, The ortho-semi-torsional (OST) spring analogy method for 3D mesh moving boundary problems, ScienceDirect, 196, pp. 747–765, DOI: 10.1016/j.cma.2006.04.009 (2007).

[5] A. Amsden and F. Harlow, "A Simplified MAC Technique for Incompressible Fluid Flow Calculations," Journal of Computational Physics, Vol. 6, pp. 322–325 (1970).

[6] S. Yoon and A. Jameson, Lower-Upper Symmetric-Gauss-Seidel Method for the Euler and Navier-Stokes Equations, AIAA, Vol. 26, pp. 1025–1026 (1988).

[7] H. A. van der Vorst, "Bi-CGSTAB: A Fast and Smoothly Converging Variant of Bi-CG for the Solution of Nonsymmetric Linear Systems," SIAM Journal on Scientific Computing, Vol. 13-2, pp. 631–644 (1992).

[8] Y. Ito and K. Nakahashi, Surface Triangulation for Polygonal Models Based on CAD Data, Internal Journal for Numerical Methods in Fluids, Vol. 39, Issue 1, pp. 75–96 (2002).